Acta Crystallographica Section B
Structural Science
ISSN 0108-7681

A five-dimensional structural investigation of the misfit layer compound $[Bi_{0.87}SrO_2]_2[CoO_2]_{1.82}$

H. Leligny,* D. Grebille, O. Pérez, A. C. Masset, M. Hervieu and B. Raveau

Laboratoire CRISMAT (UMR CNRS 6508), ISMRA, 6 Bd du Maréchal Juin, 14050 Caen, France

Correspondence e-mail: h.leligny@crismat.ismra.fr

Received 11 March 1999
Accepted 1 October 1999

The structure of the misfit layer compound $[Bi_{0.87}SrO_2]_2[CoO_2]_{1.82}$, bismuth strontium cobaltite, was determined by single-crystal X-ray diffraction using the five-dimensional superspace-group formalism. This composite crystal, of monoclinic symmetry, is composed of two subsystems exhibiting incommensurate periodicities along **b**, the binary axis direction. The first composite part $[Bi_{0.87}SrO_2]$ displays an intrinsic modulation of planar monoclinic type characterized by the wavevector $\mathbf{q}^* = 0.293\mathbf{a}^* + 0.915\mathbf{c}^*$. The second composite part $[CoO_2]$ shows two different centered lattice variants. The structure of the misfit layer crystal can be described as an alternation along **c** of distorted rock-salt-type slabs, formed from [BiO] and [SrO] layers (first subsystem), and of $[CoO_2]$ layers (second subsystem) displaying a distorted CdI_2-type structure. Two main structural results are obtained. First, as a consequence of the intrinsic modulation, disordered zones, characterized by Bi vacancies, are regularly distributed in the [BiO] layers. Second, strong chemical bonds are implied between the strontium atoms of the first subsystem and the oxygen atoms of the second one.

1. Introduction

The large family of Bi-based superconductors $Bi_2Sr_2Ca_{n-1}Cu_nO_{(2n+4+\delta)}$ (Raveau *et al.*, 1991; Tarascon *et al.*, 1991) offers a wide range of interesting structural features related to incommensurate or commensurate modulations. Similar structures have also been stabilized by substitution of Cu for another transition metal *M* (Tarascon *et al.*, 1989; Tarascon *et al.*, 1990). For example, 2201-type oxides with *M* = Cu, Co, Fe or Mn have been accurately described as modulated phases (Matsui *et al.*, 1988; Leligny *et al.*, 1992; Jakubowicz *et al.*, 1999). The corresponding modulations have been explained by the accommodation of a lattice parameter mismatch between alternate rock-salt-type slabs (RSS) [BiO–SrO] and perovskite-type layers $[MO_2]$ in relation to non-stoichiometry of oxygen or cations. In the Bi–Sr–Cu–O system, two intermodulated composite structures were determined (Frost Jensen, Larsen *et al.*, 1997; Frost Jensen, Petříček *et al.*, 1997) and were described as the stacking of two incommensurately related lattices with independent cationic frames, $[CuO_2]$ and $[(Sr_{1-x}Bi_x)_2Cu_2O_3]$, respectively.

The Bi–Sr–Co–O system has also been studied recently and novel structures have been described (Pelloquin, Masset, Maignan, Hervieu *et al.*, 1999; Pelloquin, Masset, Maignan, Michel *et al.*, 1999). In particular, two of them (Hervieu *et al.*, 1999) clearly present the structural characteristics of pure misfit layer compounds. A structural model has been proposed

Table 1
Details of data collection.

Chemical formula	$[Bi_{0.868(2)}SrO_2]_2[CoO_2]_{1.820(1)}$
Crystal size (mm)	0.250 × 0.080 × 0.0016
Crystal shape	$(\bar{1}00)$ $(4\bar{1}0)$ (010) $(0\bar{1}0)$ (001) $(00\bar{1})$
Cell parameters in Å (T = 294 K)	
First subsystem	$\mathbf{a}_{11} = 4.905\,(2)$, $\mathbf{a}_{12} = 5.112\,(1)$, $\mathbf{a}_{13} = 29.857\,(5)$, $\beta_1 = 93.45\,(2)^\circ$
Second subsystem	$\mathbf{a}_{21} = 4.904\,(1)$, $\mathbf{a}_{22} = 2.8081\,(5)$, $\mathbf{a}_{23} = 29.864\,(5)$, $\beta_1 = 93.49\,(2)^\circ$
Modulation vector	
$\mathbf{q}_{11}$	$0.293\,(2)\mathbf{a}_{11}^* + 0.915\,(9)\mathbf{a}_{13}^*$
$\mathbf{q}_{12}$	$1.8204\,(5)\mathbf{a}_{12}^*$
Superspace group	$I2/a$ (α 0 γ, 0 μ 0) pmm
Z	4
ρ (g cm^{-3}), μ (cm^{-1})	6.82, 616
Wavelength (Å)	0.71073
θ_{max} (°), $(\sin\theta/\lambda)_{max}$	45, 0.995
Scan mode	Ω, $\theta/3$

Class of reflections	Registered space	Number of measured reflections
$HKL00$	$-9 \le H \le 9, 0 \le K \le 10, -58 \le L \le 58$	6115
$HKLM_1 0$	$0 \le H \le 9, 0 \le K \le 10, -59 \le L \le 59, 1 \le \lvert M_1\rvert \le 2$	12 196
$H0L0M_2$	$-9 \le H \le 9, -58 \le L \le 58, 0 \le M_2 \le 5$	3409

Internal consistency factor R_{int} (after absorption correction)	
Subsystem (I) ($HKL00$ reflections)	0.0229
Subsystem (II) ($H0L0M_2$ reflections)	0.0278
Extremal transmission factors	0.02, 0.36

	Number of unique reflections (with $I \ge 3\sigma_I$)	Corresponding reliability factors (R/wR)
$HKLM_1M_2$	2170	0.0404/0.0346
$HKL00, K \neq 0$	878	0.0339/0.0266
$H0L00$	156	0.0292/0.0210
$HKL \pm 10$	803	0.0426/0.0381
$HKL \pm 20$	100	0.1088/0.0887
$H0L0M_2$	271	0.0817/0.0778

Number of refinement parameters	74
Weighting scheme	$1/\sigma_F^2$
$\Delta\rho_{min}$ (e Å^{-3})	−4.8
$\Delta\rho_{max}$ (e Å^{-3})	4.1
F(000)	1321

where three-atom thick $[(Sr_{1-x}Bi_x)O]_\infty$ layers with a distorted RSS are intercalated between single pseudohexagonal (HL) $[CoO_2]_\infty$ layers of edge-sharing CdI_2-type octahedra. These Bi-based composite structures are closely related to the misfit layered chalcogenides $(MX)_{1+x}(TX_2)_m$, a class of materials which are important for their crystal chemistry as well as their physical properties (Rouxel, 1996; Wiegers & Meerschault, 1992), and to the recently reported misfit layered cobaltite Tl_α $[(AO)]_{1+x}[CoO_2]$, with A = Ca and Sr (Boullay *et al.*, 1996, 1998).

In all these compounds different types of layer stackings are possible and two types of slabs are observed systematically, each one corresponding to a subsystem. These two composite parts display incommensurate periods along only one direction. In some cases, additional intrinsic modulations were observed, either in the misfit direction $(BiSe)_{1.10}(NbSe_2)$ (Zhou *et al.*, 1992) or in the layer planes $(SbS)_{1.15}(TiS_2)_m$ (Ren *et al.*, 1995, 1996). The structural study of the latter compounds was developed using a (3 + 2)-dimensional superspace approach. The origin of the intrinsic modulations lies in the incommensurate ordering of (Sb or Bi)/(S or Se) atoms in the rock salt layer.

In this paper we report the structural study of a new misfit layer compound $[Bi_{0.87}SrO_2]_2[CoO_2]_{1.82}$ exhibiting an intrinsic modulation and carried out using the (3 + 2) superspace-group formalism.

2. Experimental

2.1. Synthesis

Samples were prepared from mixtures of Bi_2O_3, SrO_2 and Co^0 in the ratio 0.75:2.5:1, pressed in the form of bars and sealed in an evacuated silica tube. The temperature was increased up to 1197 K over 6 h, maintained for 12 h and decreased down to room temperature (6 h).

2.2. Transmission electron microscopy and EDS analysis

For the electron diffraction (ED) characterization, two of the single crystals selected for the X-ray diffraction study were crushed in alcohol and the small flakes deposited on a holey carbon film supported by a copper grid. The study was carried out, using a Jeol 200 CX microscope fitted with an eucentric goniometer (± 60°) and equipped with an energy-dispersive spectroscopy (EDS) analyser.

In parallel to the X-ray diffraction study, coupled electron diffraction–EDS analyses have been carried out. The analysis of ∼13 flakes confirmed that the composition of the single crystal is homogeneous and, on average, corresponds to the actual cation ratios Bi/Sr ≃ 0.92, Bi/Co ≃ 1, leading to the approximate formula $Bi_{1.85}Sr_2Co_{1.85}$ calculated for two Sr atoms per unit.

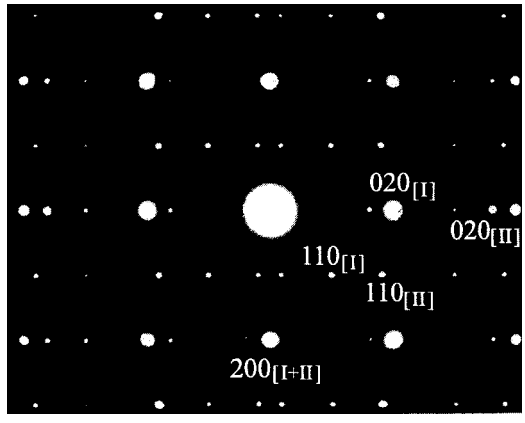

Figure 1
Electron diffraction pattern of the composite crystal ([001] zone axis); the indices of some reflections are given; the symbols I and II refer to the first and second subsystems, respectively.

The sample shows a highly lamellar character and the ED analysis confirmed the existence of two subsystems (see below). The reconstruction of reciprocal space was carried out by tilting around the crystallographic axes. It showed that the intensities of the satellite reflections resulting from the mutual modulation of both subsystems are weak. Contrary to the 2201-type oxides $Bi_2Sr_2CoO_{6+\delta}$ and $BiSr_3CoO_{6+\delta}$, and to the composite $Bi_{0.35}(Sr_{0.74}Bi_{0.26}O)_{1.72}CoO_{6+\delta}$, no flakes with the **c** axis perpendicular to the electron beam have been observed, owing to lamellae systematically oriented along (001). Another difference from the latter compounds is that very few twinning phenomena have been detected.

2.3. X-ray diffraction

The crystal quality of the samples was first checked from Weissenberg photographs. A preliminary study of the symmetry of the misfit compound was performed from precession photographs. It showed the existence of two subsystems of monoclinic symmetry, one of these subsystems displaying an intrinsic one-dimensional modulation.

A single crystal, showing sharp diffraction spots and of platelet shape ($0.250 \times 0.080 \times 0.0016$ mm^3), was selected for X-ray diffraction experiments. These sharp spots are at the nodes of two interpenetrating reciprocal lattices showing the existence of two subsystems. X-ray data collection of the reflection intensities was carried out with graphite-monochromated Mo $K\overline{\alpha}$ radiation (λ = 0.71073 Å) on an Enraf–Nonius CAD-4 diffractometer. The cell parameters of the two subsystems were refined independently from standard techniques; the $\mathbf{a}^*$ and $\mathbf{c}^*$ components of the modulation wavevector, characterizing the intrinsic modulation of the first subsystem, were refined by least-squares using the measured θ values of 43 first-order satellite reflections. The reflection intensities of the two subsystems, main reflections and satellite reflections up to second order for the first composite part and main reflections for the second one, were registered separately. No 'true satellite reflections', expected in this type of compound owing to the interactions between the subsystems, could be detected during the data collection. Corrections for Lorentz and polarization effects were applied to the data set. No significant intensity variation higher than 2% was observed for the three standard reflections chosen for each subsystem during the experiment. Absorption corrections, based on crystal morphology and using a Gaussian integration method, were applied to the reflection intensities of the two subsystems with the *JANA*98 program (Petříček & Dušek, 1998). Crystal data and experimental results are given in Table 1.

3. Symmetry

X-ray and electron diffraction patterns strongly suggest that the crystal studied has a composite structure of monoclinic symmetry comprising two subsystems (Fig. 1) having incommensurate periods along [010]. The cell parameters of the subsystem ν are denoted $\mathbf{a}_{\nu,i}$, with ν = 1 or 2 and i = 1–3. The subsystem, exhibiting spots of the largest intensity, was chosen as the reference ($\nu = 1$) to describe the crystal symmetry. This composite part exhibits an intrinsic incommensurate modulation of the planar monoclinic type (de Wolff *et al.*, 1981) with $\mathbf{q}_{11}{}^* = 0.293\,(2)\mathbf{a}_{11}{}^* + 0.915\,(9)\mathbf{a}_{13}{}^*$. Some first- and second-order satellite reflections are clearly observed on the reciprocal plane $(010)^*$ (Fig. 2), where the main spots correspond to common main reflections for the two lattices. *I* and *C* lattices are observed for the first and the second subsystem, respectively.

From the symmetry point of view, however, the two *I* and *C* lattices, with the same cell parameters $\mathbf{a}_{\nu,3}$, are not consistent, as explained hereafter. Neglecting momentarily the satellite reflections caused by the intrinsic modulation, the expression of the diffraction vector is $\mathbf{s}^* = h\mathbf{a}_{11}{}^* + k\mathbf{a}_{12}{}^* + l\mathbf{a}_{13}{}^* + M\mathbf{q}_{12}{}^*$; the fourth reciprocal vector is chosen as $\mathbf{q}_{12}{}^* = \mathbf{a}_{22}{}^* + \mathbf{a}_{21}{}^*$ ($\mathbf{a}_{21}{}^* = \mathbf{a}_{11}{}^*$), since the main reflections of the second subsystem are to be considered as satellite reflections of *M*th order of the *h*0*l* reflections related to the first subsystem (Yamamoto, 1992). Then $\mathbf{s}^* = H\mathbf{a}_{11}{}^* + K\mathbf{a}_{12}{}^* + L\mathbf{a}_{13}{}^* + M\mathbf{a}_{22}{}^*$ with $H = h + M$, $K = k$, $L = l$. It follows that the main reflections of the first and second subsystems are labelled *HKL*0 and *H*0*LM*, respectively, within this description, while *HKLM* denotes the satellite reflections owing to the mutual influence of the two composite parts.

It turns out that the condition *hkl*: $h + k + l = 2n$ related to the *I* lattice of the first subsystem leads to the condition *HKLM*: $H + K + L + M = 2n$. In particular, for the main reflections of the second subsystem, the condition *H*0*LM*: $H + L + M = 2n$ would be implied instead of the observed condition *H*0*LM*: $H + M = 2n$.

However, for the second subsystem two classes of reflections can be distinguished from a careful observation of the

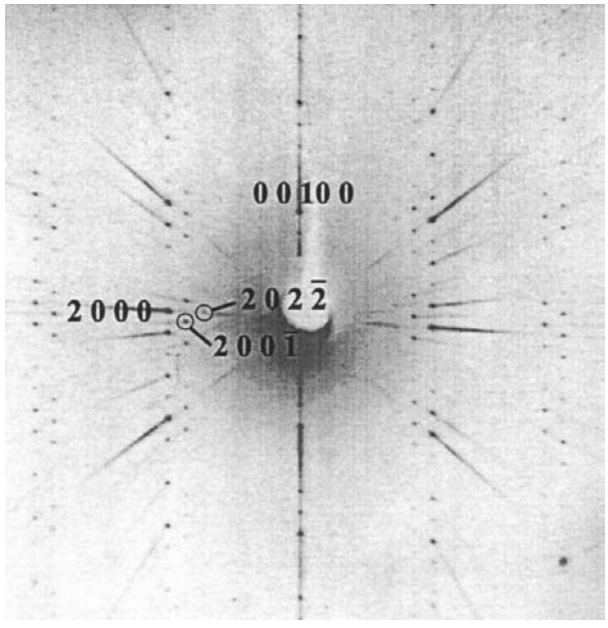

Figure 2
X-ray precession photograph [(010) plane, zero level] showing the satellite reflections of the first composite part (intrinsic modulation). Note that the main and satellite reflections draw locally a pseudo-hexagonal pattern.

diffraction pattern (Fig. 3). The first one, characterized by the largest intensities, is compatible with an F lattice with $\mathbf{a}_{23} = \mathbf{a}_{13}$, while the second one, with weaker intensities, involves a C lattice with $\mathbf{a}_{23}{}' = \mathbf{a}_{13}/2$. As a result, the main reflections of the second subsystem could be explained from the coexistence of two lattice variants inside the crystal. Then, three groups of reflections can be distinguished within the previous classes: the first one with H, M odd and L even, belonging to the C lattice only, the second one with H, M and L odd, belonging to the F lattice only, and the third one with H, M and L even, which are common reflections to both lattices. This hypothesis of two lattice variants can explain the apparent anomaly previously mentioned.

To scrutinize the compatibility between the centering conditions of the two composite lattices, let us consider separately the two variants of the second subsystem. The first (F lattice) leads us to choose as modulation vector $\mathbf{q}_{12}{}^* = \mathbf{a}_{22}{}^* + \mathbf{a}_{21}{}^* + \mathbf{a}_{23}{}^*$; then, the I lattice of the first composite part implies the condition $HKLM$: $H + K + L = 2n$ and $H0LM$: $H + L = 2n$ for the main reflections of the second composite part. Obviously, this last condition is not restrictive enough for an F lattice. Rather it is characteristic of a B lattice assuming a small lowering of the translational symmetry from F to B, although no supplementary reflections are observed. The two I and B lattices are then consistent and the modulation vector becomes $\mathbf{q}_{12}{}^* = \mathbf{a}_{22}{}^*$.

The second variant (C lattice with $\mathbf{a}_{23}{}' = \mathbf{a}_{13}/2$) leads us to choose as modulation vector $\mathbf{q}_{12}{}^* = \mathbf{a}_{22}{}^* + \mathbf{a}_{21}{}^*$. The condition $H0LM$: $H + L + M = 2n$ is then reduced to $H + M = 2n$ ($L = 2n$) and as a result the two I and C lattices are compatible.

The space group related to the average structure of the first subsystem is found to be $I2/a$. The space groups $F2/m$ or more likely $B2/a$ ($\mathbf{a}_{23} = \mathbf{a}_{13}$) and $C2/m$ ($\mathbf{a}_{23}{}' = \mathbf{a}_{13}/2$) are deduced for the two structural variants of the second subsystem. It appears from the previous results that the periodicity along the three crystallographic axes is lost, requiring the use of the five-dimensional formalism (de Wolff *et al.*, 1981; Janssen & Janner, 1980*a*,*b*). The entire diffraction pattern of the crystal can be indexed with five integer indices $HKLM_1M_2$ with respect to a set of (3 + 2) basis vectors $\mathbf{a}_i{}^*$, i = 1–5. The first three vectors are chosen as the reciprocal of $\mathbf{a}_{11}$, $\mathbf{a}_{12}$ and $\mathbf{a}_{13}$, while $\mathbf{a}_4{}^*$ and $\mathbf{a}_5{}^*$ are identified with $\mathbf{q}_{11}{}^*$ and $\mathbf{a}_{22}{}^*$, respectively; $\mathbf{a}_{22}{}^*$, the irrational part of $\mathbf{q}_{12}{}^*$, is written as $\mathbf{q}_{12}{}^{*,i}$. The reciprocal basis vectors $\mathbf{a}_{\nu,i}{}^*$ (i = 1, 2, 3) and the modulation wavevectors $\mathbf{q}_{\nu,j}{}^{*,i}$ part (j = 1, 2) of each subsystem ν are expressed as an integral linear combination of the $\mathbf{a}_i{}^*$ *via* a 5 × 5 matrix W^ν (van Smaalen, 1992), where W^1 is the identity matrix

$$\begin{pmatrix} \mathbf{a}_{\nu,1}{}^* \\ \mathbf{a}_{\nu,2}{}^* \\ \mathbf{a}_{\nu,3}{}^* \\ \mathbf{q}_{\nu,1}{}^{*,i} \\ \mathbf{q}_{\nu,2}{}^{*,i} \end{pmatrix} = W^\nu \begin{pmatrix} \mathbf{a}_1{}^* \\ \mathbf{a}_2{}^* \\ \mathbf{a}_3{}^* \\ \mathbf{a}_4{}^* \\ \mathbf{a}_5{}^* \end{pmatrix}, \; W^2 = \begin{pmatrix} 1 & 0 & 0 & 0 & 0 \\ 0 & 0 & 0 & 0 & 1 \\ 0 & 0 & 1 & 0 & 0 \\ 0 & 0 & 0 & 1 & 0 \\ 0 & 1 & 0 & 0 & 0 \end{pmatrix}.$$

W^2 is a permutation matrix (Yamamoto, 1992) which interchanges in five-dimensional space the coordinate axes 2 and 5. The superspace group (SSG) of the subsystem ν = 1, chosen as reference one and which is also the SSG of the crystal, is determined to be $I2/a$ (α 0 γ, 0 μ 0) pmm in the case of the B lattice variant, in agreement with the observed reflection conditions $HKLM_1M_2$: $H + K + L = 2n$ and $H0LM_1$0: $H = 2n$ ($L = 2n$). In the case of the lattice variant C, the SSG is $I2/a$ (α 0 γ, 1 μ 0) pmm, in agreement with the reflection conditions $HKLM_1M_2$: $H + K + L + M_2 = 2n$, $H0LM_1$0: $H = 2n$ ($L = 2n$) and $H0L0M_2$: $L = 2n$.

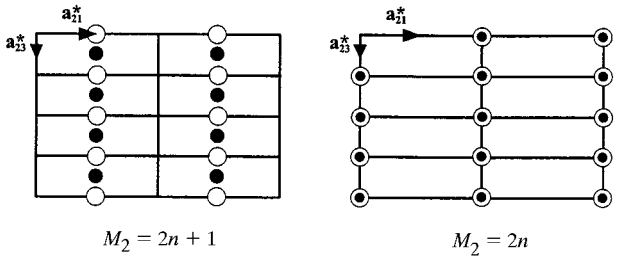

Figure 3
Schematic representation of the reciprocal space of the second subsystem. The dark and the open circles denote the reflections of the first (F) and second (C) lattice variants, respectively ($M_2 = 2n + 1$ levels); the other symbol used shows the superimposed reflections ($M_2 = 2n$ levels).

4. Structure refinements

A model for the average structure of each subsystem was established using Patterson maps calculated without the $H0L0$ common reflections and was refined from the F values with the *JANA*98 program (Petříček & Dušek, 1998). This preliminary structural study allowed us to assign the atomic species Bi, Sr, O and Co, O to the first and second composite parts, respectively. The intrinsic modulation of the first subsystem was treated in the four-dimensional approach for mono-incommensurate structures using the $HKLM_1$ reflections, except the common $H0L0$ ones. The components of the displacement vector $\mathbf{U}^\mu$ of the μth atom and the occupancy probability P^μ of the μ site by the μth atom were written as Fourier series limited to the first and second harmonics since the satellite reflections with $|M_1| > 2$ were not observed.

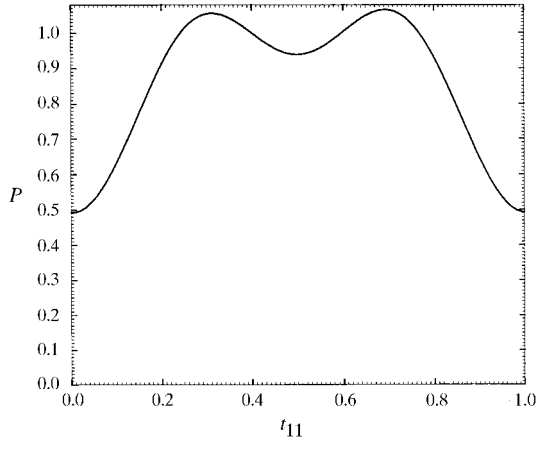

Figure 4
Occupation probability P of Bi atom *versus* the internal parameter t_{11}.

$$U_i^{\mu}(\overline{x}_4^{\mu}) = \sum_{n=1}^{2} A_{i,n}{}^{\mu} \cos 2\pi n \overline{x}_4^{\mu} + B_{i,n}{}^{\mu} \sin 2\pi n \overline{x}_4^{\mu}, \; i = 1...3$$

$$P^{\mu}(\overline{x}_4^{\mu}) = P_0{}^{\mu} + \sum_{n=1}^{2} A_n{}^{\mu} \cos 2\pi n \overline{x}_4^{\mu} + B_n{}^{\mu} \sin 2\pi n \overline{x}_4^{\mu}$$

where

$$\overline{x}_4{}^{\mu} = \mathbf{q}_{11}{}^{*} \cdot (\mathbf{r}_0{}^{\mu} + \mathbf{p}_1) = \mathbf{q}_{11}{}^{*} \cdot \mathbf{r}_0{}^{\mu} + t_{11}$$

is an internal parameter. P_0^{μ} is the average occupancy. The $\mathbf{r}_0{}^{\mu}$ parameter defines the average position of the μth atom in the origin unit cell and $\mathbf{p}_1$ is a lattice vector of the first subsystem.

A preliminary model of displacive modulation using harmonic functions was considered for all the atoms. Four-dimensional Fourier maps showed the usual undulated strings for Sr and O1 atoms belonging to the [SrO] layer. In contrast, rectilinear displacements U_1 along $\mathbf{a}_{11}$ were observed for Bi and O2 atoms located in the [BiO] layer. Consequently, the model could be improved by introducing sawtooth functions for these two atoms.

$$U_1 = 2U_{1,0}(\overline{x}_4 - \overline{x}_{4,0})/\Delta,$$

where $U_{1,0}$ is the maximum amplitude displacement along $\mathbf{a}_{11}$, $\overline{x}_{4,0}$, the midpoint corresponding to zero displacement and Δ, the width of the definition interval for the displacement function.

Anisotropic displacement parameters (ADP's: Trueblood *et al.*, 1996) were considered for Bi, Sr and isotropic ones for the O atoms. A harmonic modulation of the ADP terms was introduced for Bi. To describe the Bi occupancy, two models were tested. In the first one, the Δ value refined to 0.88, suggesting Bi vacant sites located in well defined parts of the crystal around $\overline{x}_{4,0} = 0$. In the second one, the Δ parameter was fixed at 1.0, but an occupancy modulation was assumed (Fig. 4) and described with two harmonics. This model results in partial occupation of the site even for $\overline{x}_{4,0} = 0$ and therefore implies some indeterminacy in the location of the vacant sites. It leads to a significant lowering of the reliability factors, R, mainly for R_2 related to the second-order satellite reflections: $R_G = 0.0407$, $R_0 = 0.0349$, $R_1 = 0.0435$, $R_2 = 0.1120$ against $R_G = 0.0432$, $R_0 = 0.0358$, $R_1 = 0.0471$, $R_2 = 0.1343$. R_G, R_0, R_1 and R_2 are related to: all the reflections, the main reflections (without $H0L0$ ones) and the first- and second-order satellite reflections, respectively.

Some difficulties arising from the electron density spread (Fig. 5) of the modulated string of the O2 atom were encountered during the refinement. To solve this problem, two models were considered. First, the occupancy was allowed to vary, leading to a P_0 value of $\sim$0.85; no significant modulation was observed. This model involves oxygen vacant sites within the [BiO] layers requiring the addition, in some parts of the crystal, of supplementary O atoms to complete the Bi bonding scheme. Moreover, the P_0 value seems to be artificial insofar as the whole electron density is not taken into account. In the second model, P_0 was fixed at 1.0, but, as expected, the thermal motion of the O atom is enhanced; the refined thermal parameter of O2 is consistent with the observed spread of the electron density (Fig. 5).

The three-dimensional structure refinement of the second subsystem confirmed the previous assumption concerning the existence of two variants. Indeed, considering the apparent

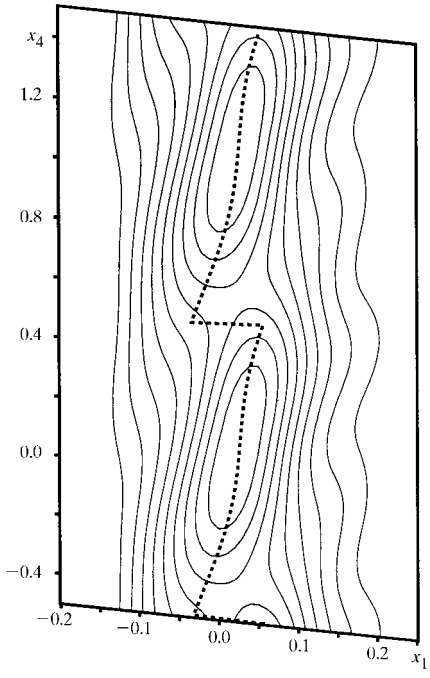

Figure 5
Section $x_1 - x_4$ of the four-dimensional difference Fourier map around the expected position of the O2 atom belonging to the [BiO] layer. The dotted line shows the considered U_1 atomic displacement function (contours at intervals of 1.25 e Å^{-3}).

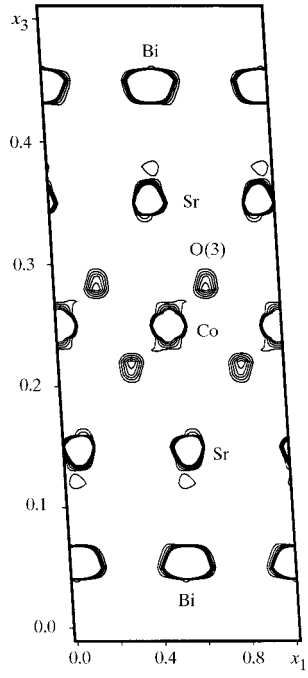

Figure 6
Observed Fourier map ([010] projection) of the composite crystal, illustrating the relative arrangement of the two subsystems (average structure). High density maxima have been artificially truncated.

space group $C2/c$ ($\mathbf{a}_{23} = \mathbf{a}_{13}$), the reflections $H0L0M_2$ with H, M_2 odd and L even, showing weaker intensities, cannot be accounted for, neither from atomic displacements (Co, O) nor from twin domains. The two variants model was checked considering an artificial P lattice ($\mathbf{a}_{23} = \mathbf{a}_{13}$) and ascertaining that the two variants have the same (or nearly the same) structure factors; three scale factors were introduced, K_1 for the specific reflections of the C lattice, K_2 for the specific reflections of the F lattice and K_3 for the even common reflections. Subsequent refinements of the model led to a reasonable R factor (0.08) and explained the intensities observed for the reflections of different parities.

Otherwise, the expected relation ${K_1}^2 + {K_2}^2 = {K_3}^2$ is verified (K_1 = 0.638, K_2 = 0.262 and K_3 = 0.671) and allows the percentage of the two lattice variants F (or B) and C to be estimated; the lattice F (or B) is found to be the main variant (83%). As the crystal studied does not exhibit a significant diffuse scattering effect along [001]*, it can be assumed that a sufficient coherence degree along [001] is established for each lattice variant.

The relative atomic positions of the two structural parts, in the [010] projection, were determined using the common $H0L0$ reflections; the calculation of a three-dimensional Fourier map, starting from the average atomic positions of the first subsystem, allowed the Co and O atoms of the [CoO_2] layers to be located (Fig. 6). A refinement was then carried out with all the reflections, considering the crystal as a composite and using the *JANA*98 program (Petříček & Dušek, 1998). Only the main B lattice variant of the second subsystem was considered. On subsequent five-dimensional Fourier maps, no significant waving of the atomic strings along x_5 (the internal axis related to the [010] misfit direction) was observed in either the first or second subsystem. Consequently, no supplementary displacement functions were introduced. The refined parameters are listed in Tables 2 and 3.

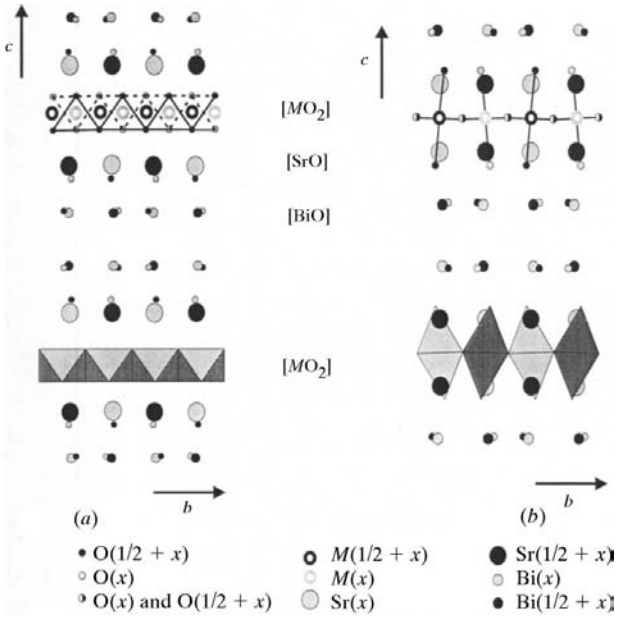

Figure 7
Compared average structures of (*a*) the misfit layer and (*b*) 2201-type compounds.

5. Discussion

5.1. The average misfit structure

The average structure of the composite crystal is depicted in Fig. 7(*a*), considering, for the [CoO_2] structural part, the main lattice variant of actual $B2/a$ symmetry. Its structure is described within the $F2/m$ enhanced symmetry, since no significant departure from the ideal value was found for the y coordinate of O3 during the refinement.

The composite structure can be described as a stacking along $\mathbf{a}_{13}$ of [SrO], [BiO] and [CoO_2] layers according to the sequence: RSS_1, HL_1, RSS_2, HL_2, RSS_1, HL_1, ..., where RSS_i represents a slab of the first composite part displaying a distorted rock-salt-type structure with the layer sequence [SrO], [BiO], [BiO], [SrO]. HL_i represents a pseudo-hexagonal layer corresponding to one [CoO_2] layer which exhibits a distorted CdI_2-type structure [$a_{21} \simeq a_{22}(3)^{1/2}$]. RSS_1 and RSS_2, and HL_1 and HL_2 are symmetry related through the respective centering condition of each subsystem.

These RSS appear to be closely similar (Fig. 7*b*) to the structural slabs BiO–SrO observed in the Bi–Co and in the Bi–Cu 2201 compounds (Jakubowicz *et al.*, 1999; Leligny *et al.*, 1992). The main difference between the previous 2201-type modulated structures and the present misfit one lies in the [MO_2] layers exhibiting quite different configurations, as underlined in Fig. 7. Consequently, the O atoms belonging to the [SrO] layers, which are bound both to Bi, Sr and M atoms in the 2201 compounds, are no longer bound to the metallic atoms in the composite phase. This characteristic could explain the metric independence between the two subsystems and thus their incommensurability along $\mathbf{a}_{12}$.

The pseudo-hexagonal [CoO_2] layers are built with CoO_6 octahedra sharing half of their edges with their neighbours. Quite similar Co—O bond distances, four of 1.906 (4) Å and two others of 1.917 (4) Å are observed, although the CoO_6 octahedra are strongly distorted, as shown by the existence of two types of O—O distances (2.58 and 2.82 Å). This distortion of the oxygen framework can be explained by the repulsions between the nearest-neighbour Co atoms and, as a result,

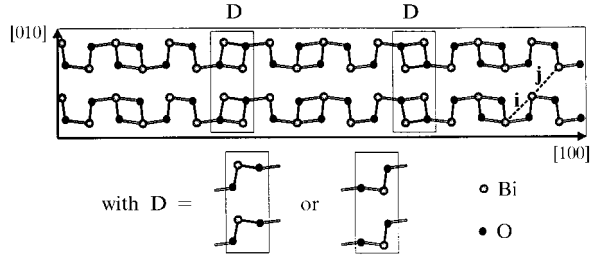

Figure 8
View of a modulated [BiO] layer pointing out the [100] Bi—O double chains. The strong (2–2.2 Å) and the intermediate (2.2–2.4 Å) Bi—O bonds are symbolized by dark and grey segments, respectively. The disordered **D** regions are framed.

Table 2
Crystallographic parameters.

Atom	Harmonic	P	x	y	z	U_{eq}/U_{iso}
Bi	0	0.868 (2)	0.0197 (3)	0.2638 (1)	0.05357 (3)	0.0158 (1)
	$\sin(2\pi\bar{x}_4)$	−0.082 (2)	0.0062 (4)	−0.0010 (4)	0.00018 (2)	
	$\cos(2\pi\bar{x}_4)$	−0.208 (2)	−0.0020 (3)	0.0004 (3)	0.00055 (3)	
	$\sin(4\pi\bar{x}_4)$	−0.098 (3)	0†	0†	0†	
	$\cos(4\pi\bar{x}_4)$	−0.116 (3)	0.0000 (0)	−0.0052 (5)	0†	
$U_{1,0} = 0.0830\,(6)$	$\Delta = 1$†	$x_4^0 = 0.551\,(2)$				
Sr	0	1†	0.0555 (1)	−0.2514 (1)	0.14851 (2)	0.0116 (1)
	$\sin(2\pi\bar{x}_4)$	0†	−0.0025 (2)	0†	0.00132 (4)	
	$\cos(2\pi\bar{x}_4)$	0†	0.0043 (2)	0†	0.00073 (4)	
O1	0	1†	0.0456 (7)	0.2337 (7)	0.1227 (1)	0.0141 (6)
	$\sin(2\pi\bar{x}_4)$	0†	−0.004 (2)	0†	0.0006 (3)	
	$\cos(2\pi\bar{x}_4)$	0†	0.008 (2)	0†	0.0012 (3)	
O2	0	1†	0.017 (2)	0.6773 (7)	0.0576 (2)	0.026 (1)
	$\sin(2\pi\bar{x}_4)$	0†	−0.007 (6)	0†	0.0016 (4)	
	$\cos(2\pi\bar{x}_4)$	0†	0.006 (3)	0†	0.0021 (5)	
$U_{1,0} = 0.046\,(7)$	$\Delta = 1$†	$x_4^0 = 0$				
Co	0	1†	0‡	0.25†	1/4‡	0.0062 (2)
O3	0	1†	−0.1787 (5)	0.75†	0.21651 (7)	0.0084 (5)

† Fixed during the refinement because their variation from the present values were not significant. ‡ Fixed because of the symmetry restraint.

prevents Co—Co bond distances which are too short to be implied in the $[CoO_2]$ layers. The bond-valence calculations (Brese & O'Keeffe, 1991) applied to cobalt lead to a mean valence state of 3.4, suggesting the coexistence of Co^{3+} and Co^{4+} species.

Assuming a full occupation of the O2 sites, the chemical formula of the composite crystal would be $[Bi_{0.87}SrO_2]_2[CoO_2]_{1.82}$; this composition appears to be consistent with the intermediate oxidation state of the Co atom and with the EDS analysis. The other model for O2, involving oxygen vacant sites in the [BiO] layers, would require a Co^{3+} valence state, inconsistent with the observed Co—O bond lengths.

5.2. The intrinsic modulation

A remarkable feature deals with the action of the intrinsic modulation on the RSS of the first composite part. As already outlined, the main modulation concerns the Bi atom. Its large rectilinear displacement along $\mathbf{a}_{11}$, correlated with its occupancy rate governed by a density wave (Fig. 4) leads to the existence of two types of zones inside each [BiO] layer; they are depicted in Fig. 8, drawn within the commensurate approximation $\mathbf{q}_{11}{}^* = 2/7\mathbf{a}_{11}{}^* + \mathbf{a}_{13}{}^*$. The first regions are characterized by a full occupancy of the sites and they build the major part of the layer. The second regions, framed and labelled **D** in Fig. 8, are disordered. Indeed, in these latter regions, half of the Bi sites, on average, are occupied by a Bi atom implying Bi vacant sites. Owing to the occupancy modulation (Fig. 4), these vacant sites are regularly distributed along $\mathbf{a}_{11}$ with approximate $7/2\mathbf{a}_{11}$ periodicity. Actually, the Bi—Bi distances between first neighbours are too short in these **D** regions (3.0–3.2 Å), requiring the existence of Bi vacancies; the local disorder involved is then explained from the existence of two possible configurations for the Bi atoms (Fig. 8).

The (010) projection of the modulated structure of the first composite part, also drawn in the commensurate approximation (Fig. 9), emphasizes the arrangement of the **D** zones in staggered rows along the stacking direction. Note also that each $[CoO_2]$ layer is inserted between two RSS, whose **D** zones are shifted by $\sim 7/4\mathbf{a}_{11}$. Otherwise, in contrast with the Bi 2201 and 2212 modulated compounds with Cu, Fe and Co (see, for example, Leligny *et al.*, 1992; Yamamoto *et al.*, 1992; Tarascon *et al.*, 1989; Jakubowicz *et al.*, 1999; Grebille *et al.*, 1996; Petříček *et al.*, 1990; Le Page *et al.*, 1989; Pérez *et al.*, 1997), no significant puckering of the [BiO] and [SrO] layers along $\mathbf{a}_{13}$ is observed in the composite crystal. This particular characteristic most probably originates from the fact that the Co atoms are only bound to the O3 atoms of the $[CoO_2]$ layers, which appear as rigid structural units.

Within one RSS, the Bi (respectively Sr) atoms are distributed in parallel cationic ribbons perpendicular to $\mathbf{a}_{11}$. Owing to the monoclinic character of the crystal, two such planes in adjacent RSS are shifted by ~0.9 Å along [100] (as shown by the dotted line in Fig. 9). This shift, along with the monoclinic symmetry, is caused by the presence of the $[CoO_2]$ layers and the distortion of their octahedra. Indeed, on each side of this layer, the Sr atom tends to be located in a position giving rise to the most symmetrical O3 environment. Running along $\mathbf{a}_{12}$, it occupies the expected median average x positions in comparison with those of the O3 atoms. A simple calculation, taking into account the distortions of the octahedra, gives for this shift a result ($\simeq$ 0.8 Å) consistent with the observed

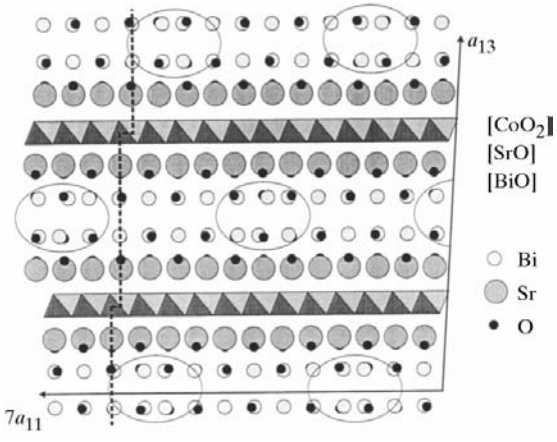

Figure 9
(010) orthogonal projection of the actual composite crystal. The disordered **D** regions are framed.

Table 3
Anisotropic displacement parameters.

	Harmonic	U_{11}	U_{22}	U_{33}	U_{12}	U_{13}	U_{32}
Bi	0	0.0210 (2)	0.0167 (2)	0.0096 (1)	0†	0.0007 (2)	0.0006 (3)
	$\sin(2\pi\bar{x}_4)$	0.0027 (3)	0.0027 (3)	0.0010 (3)	−0.0028 (3)	0.0006 (2)	0.0013 (4)
	$\cos(2\pi\bar{x}_4)$	0.0069 (4)	0.0057 (4)	0.0004 (3)	0†	−0.0005 (3)	0.0047 (9)
Sr	0	0.0093 (2)	0.0146 (2)	0.0109 (2)	0†	0.0014 (2)	0†
Co	0	0.0008 (3)	0.0075 (6)	0.0102 (3)	0‡	0.0005 (2)	0‡

† Fixed during the refinement because their variation from the present values were not significant. ‡ Fixed because of the symmetry restraint.

value. The scheme observed for the modulated structure results from the particular values of the $\mathbf{a}_{11}{}^*$ and $\mathbf{a}_{13}{}^*$ components of $\mathbf{q}_{11}{}^*$, which imply that $\mathbf{q}_{11}{}^* - \mathbf{a}_{13}{}^*$ is almost parallel to $\mathbf{a}_{11}$. Note that, considering $\mathbf{q}_{11}{}^* - \mathbf{a}_{13}{}^*$ as the modulation vector, the previous vertical planes are wave planes. Otherwise, the **D** regions form [010] ribbons which define a pseudo-hexagonal pattern. A signature of this pattern is clearly visible in Fig. 2.

5.3. The bonding scheme in the first subsystem

Two types of Bi—Bi distances are observed inside the [BiO] layers in the ordered zones. The first type ranges from 3.50 to 3.53 Å, while the second one ranges from 3.68 to 3.75 Å; they are labelled **i** and **j**, respectively, in Fig. 8. This significant difference allows each [BiO] layer to be described as a set of BiO double chains running along $\mathbf{a}_{11}$. These double chains are also characteristic of the [BiO] layers of the Bi 2201 and 2212 modulated compounds, except $Bi_2Sr_2CoO_6$ (Jakubowicz *et al.*, 1999). The interlayer Bi—Bi distances, in the ordered regions, are longer (4.00–4.1 Å), ruling out noticeable interaction between two adjacent [BiO] layers and explaining the easy cleaving of the samples.

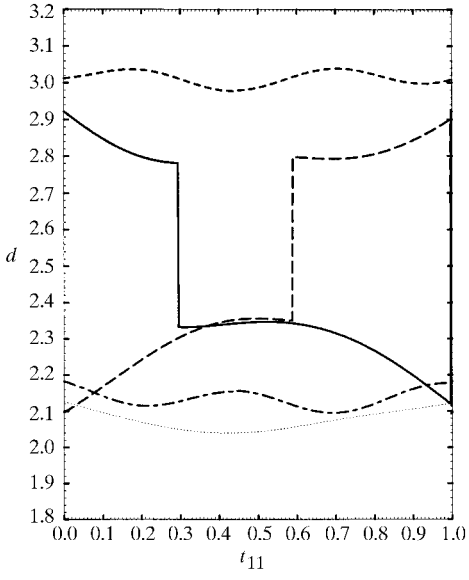

Figure 10
Variation of the interatomic Bi—O distances (Å) *versus* the internal parameter t_{11}. Bi—O1, O2, O2 ($x, y-1, z$), O2 ($\frac{1}{2}+x, 1-y, z$) and O2 ($-\frac{1}{2}+x, 1-y, z$) are represented by dotted, dot–dashed, dashed, solid and long-dashed lines, respectively.

Another interesting characteristic concerns the coordination of the Bi atom within the RSS; owing to the intrinsic modulation, this coordination is expected to vary running along $\mathbf{a}_{11}$ and $\mathbf{a}_{13}$. The Bi—O bond distance variations are plotted against the internal parameter t_{11} (Fig. 10). The Bi atom is bound to the O1 atom of the adjacent [SrO] layer and only to the O2 atoms within the same [BiO] layer, reinforcing the idea of a weak interaction between two neighbouring [BiO] layers. As expected, the Bi—O bonds roughly perpendicular to $\mathbf{a}_{11}$ (the main direction of the Bi displacements) exhibit almost constant distances (Fig. 10). In contrast, the Bi—O2 distances stretched along $\mathbf{a}_{11}$ present large variations and local discontinuities. Note that these discontinuities strongly depend on the model chosen to describe the displacive modulations of Bi and O2 atoms. As a consequence, three main types of Bi—O bonding scheme are involved. For $-0.1 \leq t_{11} \leq 0.1$, *i.e.* in the **D** regions, three short (2.1–2.2 Å) and two long ($\simeq$ 2.9 and 3.0 Å) distances are observed. The Bi coordination polyhedron can be described as a distorted tetrahedron, where the Bi lone pair occupies one of the apices. For $0.3 \leq t_{11} \leq 0.6$, two short (~2.00 and 2.15 Å), two intermediate (~2.35 Å) and one long (~3.0 Å) distances are involved. The Bi coordination polyhedron is a somewhat distorted trigonal bipyramid, where the Bi lone pair and the two O atoms strongly bonded to Bi occupy the apices of the triangular base. Between these two t_{11} intervals, an intermediate situation is observed. These different Bi—O bonding schemes, which imply a strong stereoactivity of the $6s^2$ lone pair of Bi^{3+}, are quite similar to those reported previously (Jakubowicz *et al.*, 1998). The calculation of the Bi—O bond valences (Brese & O'Keeffe, 1991) leads to values (from 2.8 to 3.1) consistent with the Bi^{3+} valence state for the whole environment. Note that a difference with the Bi 2201 and 2212 modulated phases is observed. Bi vacancies are found in the **D** regions of the composite crystal and locally two possible Bi configurations are involved (Fig. 8). The corresponding disordered regions of the 2201 or 2212 phases do not show Bi vacancies, but rather a small splitting of the Bi site with the occurrence of a specific oxygen site. The spread of the electron density observed for O2 could be explained assuming a relaxation of the position of this atom in the disordered **D** regions. A similar hypothesis could be proposed to explain the large ADP terms of the Bi atom in these zones.

Table 4 lists the Sr—O1 and Sr—O2 bond distances of the first composite part; five bond distances are involved, showing small variations throughout the crystal.

5.4. The interbonding subsystems

A remarkable result concerns the existence of strong interactions between the two composite parts of the crystal *via* Sr—O3 bonds. This property is illustrated in Fig. 11, which shows the variations of the Sr—O3 distances (d) as a function

Table 4
Sr—O distances ($\sigma \simeq 0.005$ Å) in the first subsystem.

	d_{min} (Å)	d_{max} (Å)
Sr—O1^{i}	2.536	2.608
Sr—O1^{ii}	2.562	2.589
Sr—O1	2.590	2.609
Sr—O2^{iii}	2.688	2.726
Sr—O1^{iii}	2.736	2.752

Symmetry codes: (i) $-\frac{1}{2}+x, -y, z$; (ii) $\frac{1}{2}+x, -y, z$; (iii) $x, -1+y, z$.

of t_{22}, the internal parameter corresponding to the [010] misfit direction, and defined by $t_{22} = \mathbf{q}_{22}^{*} \cdot \mathbf{p}_2$, where $\mathbf{p}_2$ is a lattice vector of the second subsystem. The different curves on Fig. 11 have been drawn for $t_{11} = 0$, *i.e.* in the vicinity of the **D** zones. The minimum values (d_m) of the Sr—O3 distances change in a significant manner with t_{11}, *i.e.* running along $\mathbf{a}_{11}$ and $\mathbf{a}_{13}$. Indeed d_m (Sr—O3) varies from 2.33 to 2.43 Å, while d_m (Sr—O3^{I}) varies from 2.31 to 2.39 Å ($\sigma \simeq 0.005$ Å). Note that the particular value $t_{11} = 0$ leads to the shortest Sr—O3 distances.

From the curves $d(t_{22})$ determined for $t_{11} = 0$ (in the **D** zones) and $t_{11} = 0.5$ (in the ordered zones) it is possible to specify, in these two cases, the bonding scheme along the [010] misfit direction. The corresponding Sr—O3 distances are listed in Table 5. As $6 \times \mathbf{a}_{12}$ is roughly equal to $11 \times \mathbf{a}_{22}$, only six unit cells along [010], refering to the first subsystem, have been considered to determine the Sr—O3 distances. It appears that, for each Sr atom, at least one strong Sr—O3 bond is implied with d ranging from 2.3 to 2.5 Å (Table 5). Otherwise, for $t_{11} = 0.5$ (in the ordered zones), the calculated Sr valence state (Table 5) is in agreement with the expected value, while it deviates in a noticeable way from the ideal value for $t_{11} = 0$ (in the **D** zones). These excessive values probably result from Sr—O3 distances which are too short. The existence of a modulation, expected in this type of crystal, owing to the mutual influence of the two subsystems, would allow this anomaly to be suppressed. This possible modulation would act on O3, or on both Sr and O3, but unfortunately no 'true satellite reflections' were observed, preventing us from refining the corresponding displacement terms.

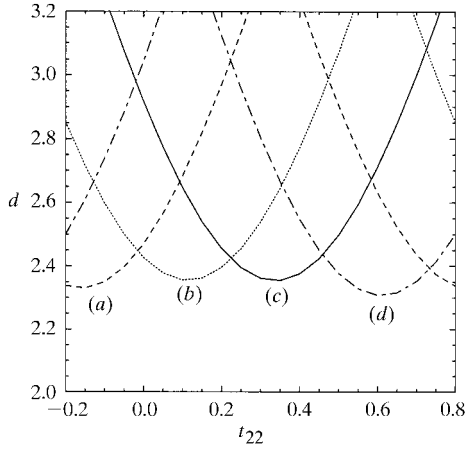

Figure 11
Variation of the Sr—O3 distances (Å) as a function of t_{22}, illustrating the interaction bonding between the two subsystems. The curves labelled (*a*), (*b*), (*c*) and (*d*) are related to the distances Sr^{ii}—O3, Sr^{ii}—O3^{i}, Sr^{iv}—O3 and Sr^{iv}—O3^{i}, respectively, and are drawn for $t_{11} = 0$. (i) $\frac{1}{2}+X,\ 1-Y,\ Z$ (second subsystem); (ii) $\frac{1}{2}+x,\ \overline{y}, z$; (iv) $x, 1+y, z$ (first subsystem).

Table 5
Sr—O distances ($\sigma \simeq 0.005$ Å) between the two subsystems.

The distances in bold are related to Sr^{iv}—O3^{I} bonds, the remainder correspond to Sr^{iv}—O3 bonds. Symmetry codes: (iv) $x, 1+y, z$ (first subsystem); (I) $\frac{1}{2}+X, 1-Y, Z$ (second subsystem).

	n_{12}					
Distances (d, Å) and valence (Σs)	0	1	2	3	4	5
$t_{11} = 0$						
d	**2.33**	**2.32**	**2.42**	2.38	2.39	**2.38**
	2.60	2.63	2.45	**2.60**	**2.55**	2.50
	2.90	2.84		**2.80**	**2.90**	
Σs	2.23	2.25	2.13	2.20	2.19	2.13
$t_{11} = 0.5$						
d	**2.40**	**2.40**	**2.48**	2.44	2.45	**2.45**
	2.67	2.72	2.53	**2.67**	**2.62**	2.56
	2.97	2.90		**2.87**	**2.95**	
Σs	1.99	1.99	1.90	1.97	1.97	1.91

6. Concluding remarks

This study reinforces previous results demonstrating the ability of oxides to form misfit layer compounds closely related to chalcogenides, *i.e.* involving CdI_2 and rock-salt-type layers. A fundamental property of the present oxide concerns the existence of an intrinsic modulation which is rarely observed in chalcogenides. This phenomenon has only been seen in $(BiSe)_{1.10}NbSe_2$ (Zhou *et al.*, 1992) and in $(SbS)_{1.15}(TiS_2)_m$ (Ren *et al.*, 1995; Ren *et al.*, 1996), where the modulation is of the density type. In the crystal studied the intrinsic modulation implies both atomic displacements and a probability law for the Bi site occupancies. The observed displacive modulation along [100] (no significant puckering along [001] is involved) is similar to the usual longitudinal modulations encountered in other Bi–Sr–*M*–O systems. A consequence of this intrinsic modulation is the existence, within the [BiO] layers, of Bi disordered zones with vacant sites periodically distributed in the crystal. A possible misfit modulation acting on O3, or on both Sr and O3, should perhaps be considered and would likely allow us to improve the present model.

A remarkable structural property of this oxide concerns the existence of strong Sr—O bonds between the CoO_2 and *RS*-type layers, characterized by minimum distances close to 2.40 Å. In this respect, this oxide is very similar to the cuprate $[Bi_{0.08}Sr_{1.92}Cu_2O_3]_7[CuO_2]_{10}$, whose modulated composite crystal structure (Frost Jensen *et al.*, 1997), built up of $[A_2Cu_2O_3]$ and $[CuO_2]$ layers, is also characterized by strong interlayer Sr—O bonds. Finally, the bidimensional character of the structure of this oxide is not related to the coexistence of two subsystems, but rather results from the weak interaction between the two adjacent Bi—O layers of the RSS subsystem.

The authors are greatly indebted to Dr V. Petříček for providing *JANA*98 with the necessary modifications and to Mrs J. Chandon for the technical assistance.

References

Boullay, Ph., Domengès, B., Hervieu, M., Groult, D. & Raveau, B. (1996). *Chem. Mater.* **8**, 1482–1489.

Boullay, Ph., Sheshadri, R., Studer, F., Hervieu, M., Groult, D. & Raveau, B. (1998). *Chem. Mater.* **10**, 92–102.

Brese, N. E. & O'Keeffe, M. (1991). *Acta Cryst.* B**47**, 192–197.

Frost Jensen, A., Larsen, F. K., Iversen, B. B., Petříček, V., Schultz, T. & Gao, Y. (1997). *Acta Cryst.* B**53**, 113–125.

Frost Jensen, A., Petříček, V., Larsen, F. K. & McCarron, E. M. (1997). *Acta Cryst.* B**53**, 125–134.

Grebille, D., Leligny, H., Ruyter, A., Labbé, Ph. & Raveau, B. (1996). *Acta Cryst.* B**52**, 628–642.

Hervieu, M., Boullay, Ph., Michel, C., Maignan, A., Hervieu, M. & Raveau, B. (1999). *J. Solid State Chem.* **142**, 305–318.

Jakubowicz, N., Grebille, D., Leligny, H. & Evain, M. (1999). *J. Phys.* **11**, 3997–4008.

Jakubowicz, N., Pérez, O., Grebille, D. & Leligny, H. (1998). *J. Solid State Chem.* **139**, 194–199.

Janssen, T. & Janner, A. (1980*a*). *Acta Cryst.* A**36**, 399–408.

Janssen, T. & Janner, A. (1980*b*). *Acta Cryst.* A**36**, 408–415.

Leligny, H., Durčok, S., Labbé, Ph., Ledésert, M. & Raveau, B. (1992). *Acta Cryst.* B**48**, 407–418.

Le Page, Y., McKinnon, W. R., Tarascon, J. M. & Barboux, P. (1989). *Phys. Rev. B*, **40**, 6810–6816.

Matsui, Y., Takekawa, S., Horiuchi, S. & Umezono, A. (1988). *Jpn J. Appl. Phys.* **27**, L1873–L1876.

Pelloquin, D., Masset, A. C., Maignan, A., Hervieu, M., Michel, C. & Raveau, B. (1999). *J. Solid State Chem.* **148**, 108–118.

Pelloquin, D., Masset, A. C., Maignan, A., Michel, C., Hervieu, M. & Raveau, B. (1999). *Chem. Mater.* **11**, 84–89.

Pérez, O., Leligny, H., Grebille, D., Grenêche, J. M., Labbé, Ph., Groult, D. & Raveau, B. (1997). *Phys. Rev. B*, **55**, 1236–1246.

Petříček, V. & Dušek, M. (1998). *JANA*98. Institute of Physics, Academy of Sciences of the Czech Republik, Prague.

Petříček, V., Gao, Y., Lee, P. & Coppens, P. (1990). *Phys. Rev. B*, **42**, 4228–4239.

Raveau, B., Michel, C., Hervieu, M. & Groult, D. (1991). *Crystal Chemistry of High T_c Superconductive Cuprates.* Berlin: Springer Verlag.

Ren, Y., Meetsma, A., Petříček, V., van Smaalen, S. & Wiegers, G. A. (1995). *Acta Cryst.* B**51**, 275–287.

Ren, Y., Meetsma, A., Wiegers, G. A. & van Smaalen, S. (1996). *Acta Cryst.* B**52**, 389–397.

Rouxel, J. (1996). *C. R. Acad. Sci.* **323-1(b)**, 41–57.

Smaalen, S. van (1992). *Incommensurate Sandwiched Layered Compounds*, edited by A. Meershaut, pp. 173–222. Aedermannsdorf, Switzerland: Trans. Tech. Pub.

Tarascon, J. M., Le Page, Y., McKinnon, W. R., Ramesh, R., Eibschutz, M., Tselepis, E., Wang, E. & Hull, G. W. (1990). *Eur. J. Solid State Inorg. Chem.* **27**, 81.

Tarascon, J. M., McKinnon, W. R. & Le Page, Y. (1991). *Chemistry of High Temperature Superconductors*, edited by C. N. R. Rao, p. 186. World Scientific Publishing Corporation.

Tarascon, J. M., Miceli, P. F., Barboux, P., Hwang, D. M., Hull, G. W., Giroud, M., Greene, L. H., Le Page, Y., McKinnon, W. R. & Tselepis, E., Pleizier, G., Eibscutz, M., Neumann, D. A. & Phyne, J. J. (1989). *Phys. Rev. B*, **39**, 11587–11598.

Trueblood, K. N., Burgi, H. B., Burzlaff, H., Dunitz, J. D., Gramaccioli, C. M., Schulz, H. H., Shmueli, U. & Abrahams, S. C. (1996). *Acta Cryst.* A**52**, 770–781.

Wiegers, G. A. & Meerschault, A. (1992). *J. Alloys Compd*, **178**, 351–368.

Wolff, P. M. de, Janssen, T. & Janner, A. (1981). *Acta Cryst.* A**37**, 625–636.

Yamamoto, A. (1992). *Acta Cryst.* A**48**, 476–483.

Yamamoto, A., Takayama-Muromachi, E. & Izumi, F. (1992). *Physica C*, **201**, 137–144.

Zhou, W. Y., Meetsma, A., de Boer, J. L. & Wiegers, G. A. (1992). *Mater. Res. Bull.* **27**, 563–572.